A Dynamic Mathematical Model for Monoclonal Antibody N-Linked Glycosylation and Nucleotide Sugar Donor Transport Within a Maturing Golgi Apparatus

Ioscani Jimenez del Val, Judit M. Nagy, and Cleo Kontoravdi
Dept. of Chemical Engineering and Chemical Technology, Imperial College London, South Kensington Campus, London SW7 2AZ, U.K.

DOI 10.1002/btpr.688
Published online September 28, 2011 in Wiley Online Library (wileyonlinelibrary.com).

Monoclonal antibodies (mAbs) are one of the most important products of the biopharmaceutical industry. Their therapeutic efficacy depends on the post-translational process of glycosylation, which is influenced by manufacturing process conditions. Herein, we present a dynamic mathematical model for mAb glycosylation that considers cisternal maturation by approximating the Golgi apparatus to a plug flow reactor and by including recycling of Golgi-resident proteins (glycosylation enzymes and transport proteins [TPs]). The glycosylation reaction rate expressions were derived based on the reported kinetic mechanisms for each enzyme, and transport of nucleotide sugar donors [NSDs] from the cytosol to the Golgi lumen was modeled to serve as a link between glycosylation and cellular metabolism. Optimization-based methodologies were developed for estimating unknown enzyme and TP concentration profile parameters. The resulting model is capable of reproducing glycosylation profiles of commercial mAbs. It can further reproduce the effect gene silencing of the FucT glycosylation enzyme and cytosolic NSD depletion have on the mAb oligosaccharide profile. All novel elements of our model are based on biological evidence and generate more accurate results than previous reports. We therefore believe that the improvements contribute to a more detailed representation of the N-linked glycosylation process. The overall results show the potential of our model toward evaluating cell engineering strategies that yield desired glycosylation profiles. Additionally, when coupled to cellular metabolism, this model could be used to assess the effect of process conditions on glycosylation and aid in the design, control, and optimization of biopharmaceutical manufacturing processes. © 2011 American Institute of Chemical Engineers *Biotechnol. Prog.*, 27: 1730–1743, 2011
Keywords: N-linked glycosylation, Golgi cisternal maturation, dynamic mathematical modeling, monoclonal antibodies, nucleotide sugars

Introduction

Monoclonal antibodies (mAbs) are currently the highest selling products of the biopharmaceutical industry.[1] Almost all commercial mAbs are based on the immunoglobulin (IgG) isotype.[2] All IgG-based mAbs contain a consensus N-linked glycosylation site on the Cγ2 domains of their heavy chains.[2] Many studies have found that the oligosaccharides attached to these sites greatly influence the efficacy of mAbs as therapeutics either by reducing their serum half-life[3,4] or by directly affecting the therapeutic mechanisms they trigger in the patient.[2,5] mAbs are produced industrially by culturing mammalian cells and it has been widely reported that cell culture conditions affect protein glycosylation,[6–8] thus having great impact on their end quality.

Recently, the US Food and Drug Administration and the European Medicines Agency have proposed implementing the Quality by Design (QbD) paradigm to the manufacture of biopharmaceuticals.[9] Implementation of QbD requires the use of all available knowledge regarding a given product, including the parameters that affect its quality, for the design, optimization and control of said manufacturing process.[9] The goal of QbD is to ensure that quality is "built into the product" at every stage of the manufacturing process.[10] It has been recently proposed that detailed mathematical models may play a critical role in the design, control and optimization of biopharmaceutical manufacturing processes under the QbD scope.[8]

To our knowledge, there are currently no mathematical models that relate mAb glycosylation with cell culture conditions. A model with this capability would be useful for bioprocess design and control, culture media formulation, and hypothesis testing for possible genetic engineering strategies. Toward this goal, we present a novel mathematical solution to describe the glycosylation process within a maturing Golgi apparatus. In addition, an initial bridge between

This article is dedicated to Dr. Judit M. Nagy.

Additional Supporting Information may be found in the online version of this article.

Correspondence concerning this article should be addressed to C. Kontoravdi at cleo.kontoravdi@imperial.ac.uk.

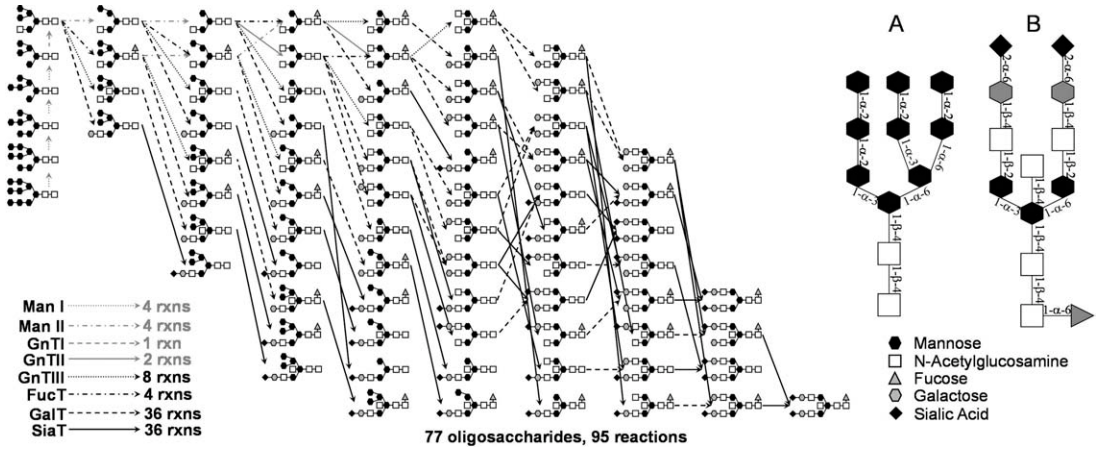

Figure 1. mAb Fc glycosylation reaction scheme and oligosaccharide linkages.

The reaction scheme consists of 77 species and 95 reactions catalyzed by eight different enzymes. A: A high mannose oligosaccharide, along with its linkages. The terminally processed biantennary oligosaccharide with its constituting linkages is presented in (B).

cellular metabolism and the glycosylation process has been established by considering the transport of nucleotide sugar donors (NSDs) from the cytosol, where they are produced, to the Golgi apparatus, where they are consumed in glycosylation reactions. The kinetic information for this model has been compiled from literature sources and model-based optimization strategies have been developed for estimation of its unknown parameters. This information has been used to simulate the model and the obtained results are compared with experimental data and with previous mathematical models.

Monoclonal Antibody N-Linked Glycosylation

All IgG-based mAbs contain a consensus N-linked glycosylation site on the constant γ-2 (Cγ2) domains of their heavy chains[2] and may also have N-linked glycosylation sites on their antigen-binding fragments (Fab), although these are relatively less common (<20%) in IgG-based antibodies.[11] The present model will only deal with constant fragment (Fc) glycans given that Cγ2 N-glycosylation is predominant in mAbs. The N-linked glycosylation process begins with the addition of a precursor nine-mannose oligosaccharide (panel A of Figure 1) to the nascent polypeptide chain in the endoplasmic reticulum (ER). Glucose residues of the protein-bound oligosaccharide assist in the correct folding of the protein, and once adequate folding has been achieved, the glycoprotein is transported to the Golgi apparatus where a series of enzymatic reactions (shown in Figure 1) sequentially convert the precursor oligosaccharide into a complex carbohydrate such as the one depicted in panel B of Figure 1.[12] The model presented here assumes that the first step of the N-linked glycosylation process is completed successfully. Hence, the model will only represent what occurs in the Golgi apparatus.

The close proximity of both Cγ2 domains in IgG molecules limits the space available for the oligosaccharide structures, thus limiting their branching and complexity.[13] Previous reports show that the oligosaccharides bound to the Fc of mAbs are limited to complex, bi-antennary structures that are usually core fucosylated, and have varying degrees of galactosylation and low levels of sialylation.[14,15] For these reasons, the reaction scheme for mAb Fc glycosylation can be limited to the one seen in Figure 1. The structure and constituting monosaccharide linkages of these oligosaccharides are presented in panels A and B of Figure 1.

Definition of the Mathematical Model

Four models of N-linked glycosylation have been formulated over the past 15 years. Shelikoff et al.[16] addressed the attachment of the precursor oligosaccharide to the nascent polypeptide in the ER, which is beyond the scope of this study. The remaining models have focused on the oligosaccharide processing reactions within the Golgi apparatus.[17–19] They considered all possible oligosaccharide processing reactions and generated insight into the N-linked glycosylation process by exploring the effects of increased protein productivity, enzyme overexpression, and luminal Golgi NSD availability. These previous models were developed to assess possible cell engineering strategies to control glycosylation, hence they included certain simplifying assumptions: they considered the same kinetic mechanism for all the sugar addition reactions and also isolated the Golgi apparatus from cell metabolism by considering constant NSD concentrations within their system. In addition, the two earlier models[18,19] considered the Golgi apparatus to be a series of static compartments connected in series. Hossler et al.[17] considered Golgi both a static system and as a series of four plug flow reactors (PFRs) to represent Golgi cisternal maturation. However, this group considered each PFR as a Golgi cisterna and did not consider Golgi resident protein recycling. We have built on the advances of these previous models and have attempted to overcome some of their limitations as will be described in this section. The three main contributions of the mathematical model presented herein are:

i. The Golgi apparatus functions under the so-called cisternal maturation regime.

ii. The individual rate expressions for the enzymatic reactions that occur within the Golgi apparatus have been derived from the kinetic mechanisms that have been reported for each enzyme.

iii. The protein-mediated transport of NSDs into the Golgi apparatus has been included to provide a link between cellular metabolism and the Golgi glycosylation process.

Cisternal maturation and material balances

Most of the current experimental information surrounding the Golgi apparatus favors the cisternal maturation model over the previously accepted static Golgi model.[20–23] Cisternal maturation postulates that the Golgi compartments are synthesized from components of the ER and transit toward the secretory components of the cell.[24,25] During their movement,

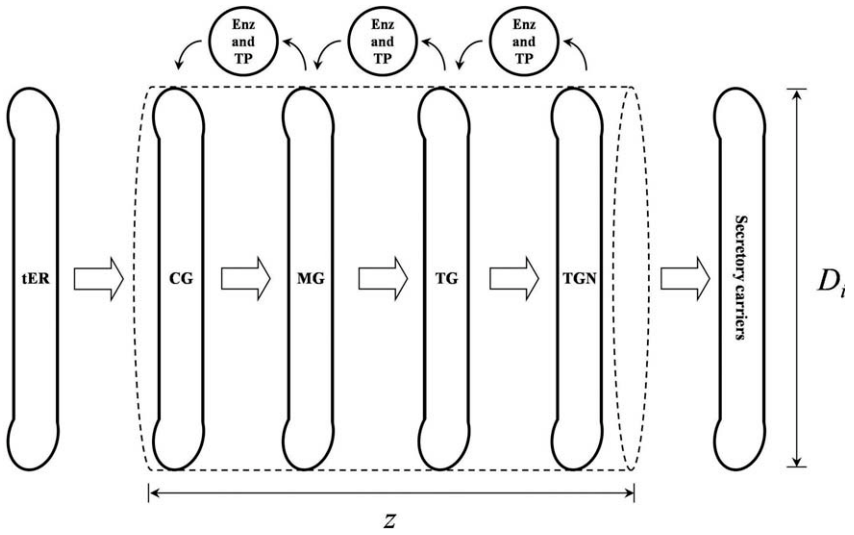

Figure 2. Cisternal maturation of the Golgi apparatus viewed as a PFR.

A single cisterna is produced from components of the endoplasmic reticulum (tER) and enters the Golgi space, which is defined herein as an imaginary tube (dotted line). The cisterna transits through the Golgi space and while this occurs, its resident proteins (TPs and glycosylation enzymes) are transported to preceding compartments as depicted by the vesicles shown at the top. Once the compartment reaches the end of the tube, its contents are transferred to carriers that are responsible for secreting glycoproteins to the extracellular environment.

Golgi-resident proteins are recycled from subsequent compartments to preceding ones through retrograde transport mediated by COPI coated vesicles.[20,23] Based on cisternal maturation, the Golgi apparatus has been modeled as a single PFR, as illustrated in Figure 2. Although the compartments are discrete sections, their movement along the z axis is continuous, thus making it possible to consider the system as a single, continuous PFR. Assuming no axial dispersion within the compartment, constant flow of cargo through the complex (constant linear velocity), no mass transfer limitations and constant diameter of the Golgi compartments, the time-dependent material balance for the components inside the PFR are shown in Eqs. 1, 2, and 3.

Oligosaccharide balances:

$$\frac{\partial \mathrm{OS}_i}{\partial t} = -\frac{4q}{\pi D_i^2}\frac{\partial \mathrm{OS}_i}{\partial z} - \sum_{j=1}^{\mathrm{N.R.}} v_{i,j} r_j \tag{1}$$

NSD balances:

$$\frac{\partial \mathrm{Pc}_k}{\partial t} = F_{k,\mathrm{in}} - \frac{4q}{\pi D_i^2}\frac{\partial \mathrm{Pc}_k}{\partial z} - \sum_{j=1}^{\mathrm{N.R.}} v_{k,j} r_j \tag{2}$$

By-product balances:

$$\frac{\partial \mathrm{B}_k}{\partial t} = -F_{k,\mathrm{in}} - \frac{4q}{\pi D_i^2}\frac{\partial \mathrm{B}_k}{\partial z} + \sum_{j=1}^{\mathrm{N.R.}} v_{k,j} r_j \tag{3}$$

An integral element of the cisternal maturation model is that the resident proteins of the Golgi apparatus (glycosylation enzymes and transport proteins [TPs]) are recycled from subsequent compartments to preceding ones.[20,23] In the present model, this has been incorporated by defining enzyme concentration profiles along the length, z, as three parameter normal functions (Eqs. 4 and 5):

Enzymes:

$$E_j(z) = E_{j,\max} exp^{-\frac{1}{2}\left(\frac{z-z_{j,\max}}{\omega_j}\right)^2} \tag{4}$$

Transport proteins:

$$\mathrm{TP}_k(z) = \mathrm{TP}_{k,\max} exp^{-\frac{1}{2}\left(\frac{z-z_{k,\max}}{\omega_k}\right)^2} \tag{5}$$

These functions represent the inherent behavior of enzyme concentration when recycling is considered: there would be a stage during which the enzyme accumulates while it is being fed into a given compartment from the subsequent one. The enzyme concentration would then reach a transitory peak concentration after which the enzyme would begin to be transferred to preceding compartments, thus generating a decline stage. The unknown parameters in Eqs. 4 and 5 are $E_{j,\max}$, ω_j, $\mathrm{TP}_{k,\max}$, ω_k and $z_{k,\max}$. $E_{j,\max}$ and $\mathrm{TP}_{k,\max}$ represent the peak concentration each of the resident proteins reach in a given Golgi cisterna. ω_j and ω_k represent the breadth of the distributions. Physically, the value of the ω parameters are associated to the ratio between the rate of forward cisternal flow and the retrograde transport of the resident proteins. If the forward flow of the cisternae is higher than that of the retrograde transport of the COPI-coated vesicles which transport the Golgi resident proteins, the concentration profiles would be broader, implying a higher value for the ωs. For the enzymes, $z_{j,\max}$, which are the position along the Golgi space where the they reach their maximum concentration, have been obtained from Ref. 26. Optimization-based methods, which will be presented in subsequent sections of this article, have been developed to estimate the unknown parameters of Eqs. 4 and 5. To our knowledge, the present model is the first instance where Golgi resident protein recycling has been considered toward describing N-linked glycosylation. We therefore believe that our approach proposes a rational and more accurate description of the phenomenon.

Enzyme kinetics

The previous models for N-linked glycosylation were based on simplified enzyme kinetics, where only competitive inhibition was considered. Moreover, they considered the

Table 1. Kinetic Mechanisms of N-Glycosylation Enzymes

Kinetic Mechanism	Reaction Mechanism	Enzymes
Michaelis Menten with competitive and product inhibitions	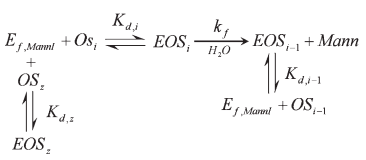	ManI[27,28] ManII[29]
Sequential-order Bi-Bi with competitive and product inhibitions	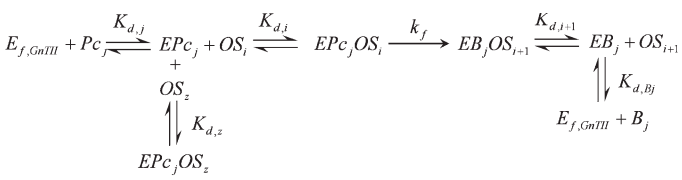	GnTI[30] GnTII[31] GalT[32]
Random-order Bi-Bi with competitive and product inhibitions	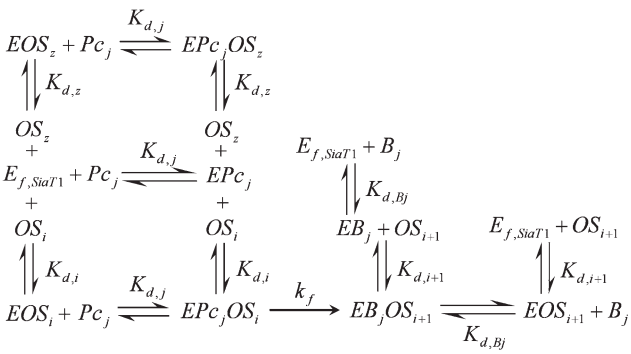	FucT[33] GnTIII[34] SiaT[35]

same kinetic mechanism for all of the enzyme-catalyzed reactions. The kinetic expressions in the present model were expanded by accounting for the structural and kinetic mechanisms by which these enzymes act.

Table 1 shows that three kinetic mechanisms prevail among the enzymes involved in mAb N-linked glycosylation. Each reaction mechanism defines how the substrate(s) bind to the enzyme, and which step of the process is the catalytic one. Additionally, but not independently to the catalytic mechanism, different types of inhibitory effects may occur within these systems. Given that many different oligosaccharides can be substrates for the same enzyme, it is reasonable to assume that competitive inhibition occurs. Moreover, product inhibition has been reported for many of these reactions.[32–34] The reaction rates are presented as Eqs. 6–8. The full derivation is included in Supporting Information (S1). Despite the modifications to the rate expressions, no additional parameters have been added compared with the previous models.

Michaelis-Menten kinetics:

$$r_j = \frac{k_{f,j}\left[E_j\right]\left[\mathrm{OS}_i\right]}{K_{d,i}\left(1 + \frac{[\mathrm{OS}_i]}{K_{d,i}} + \sum_{z=1}^{\mathrm{N.C.}} \frac{[\mathrm{OS}_z]}{K_{d,z}} + \frac{[\mathrm{OS}_{i-1}]}{K_{d,i-1}}\right)} \tag{6}$$

Sequential-order Bi-Bi kinetics:

$$r_j = \frac{k_{f,j}\left[E_j\right]\left[\mathrm{Pc}_k\right]\left[\mathrm{OS}_i\right]}{K_{d,i}K_{d,k}\left(1 + \frac{[\mathrm{Pc}_k]}{K_{d,k}} + \frac{[\mathrm{Pc}_k]}{K_{d,k}}\frac{[\mathrm{OS}_i]}{K_{d,i}} + \frac{[\mathrm{Pc}_k]}{K_{d,k}}\sum_{z=1}^{\mathrm{N.C.}} \frac{[\mathrm{OS}_z]}{K_{d,z}} + \frac{[\mathrm{B}_k]}{K_{d,\mathrm{Bk}}}\frac{[\mathrm{OS}_{i+1}]}{K_{d,i+1}} + \frac{[\mathrm{B}_k]}{K_{d,\mathrm{Bk}}}\right)} \tag{7}$$

Random-order Bi-Bi kinetics:

$$r_j = \frac{k_{f,j}\left[E_j\right]\left[\mathrm{Pc}_k\right]\left[\mathrm{OS}_i\right]}{K_{d,i}K_{d,k}\left(1 + \frac{[\mathrm{Pc}_k]}{K_{d,k}} + \frac{[\mathrm{OS}_i]}{K_{d,i}} + \sum_{z=1}^{\mathrm{N.C.}} \frac{[\mathrm{OS}_z]}{K_{d,z}} + \frac{[\mathrm{Pc}_k]}{K_{d,k}}\frac{[\mathrm{OS}_i]}{K_{d,i}} + \frac{[\mathrm{Pc}_k]}{K_{d,k}}\sum_{z=1}^{\mathrm{N.C.}} \frac{[\mathrm{OS}_z]}{K_{d,z}} + \frac{[\mathrm{B}_k]}{K_{d,Bk}}\frac{[\mathrm{OS}_{i+1}]}{K_{d,i+1}} + \frac{[\mathrm{B}_k]}{K_{d,Bk}} + \frac{[\mathrm{OS}_{i+1}]}{K_{d,i+1}}\right)} \tag{8}$$

Nucleotide sugar donor transport

NSDs (UDP-GlcNAc, GDP-Fuc, UDP-Gal and CMP-Neu5Ac) are the co-substrates for the sugar addition reactions of N-linked glycosylation and their availability inside the Golgi cisternae has been reported to affect the N-linked glycosylation process.[36–38] NSDs are synthesized in the cytosol of cells (with the exception of CMP-Neu5Ac, which is produced in the nucleus) and their transfer into the Golgi apparatus is mediated by TPs. All four TPs considered in this article, act by an antiport mechanism whereby the NSDs are transported into the Golgi cisternae while their dephosphorylated nucleotide component, which accumulates in the

Golgi lumen through the glycosylation reactions, is transported out of the cisternae.[39] For example, the TP for UDP-GlcNAc removes a single uridine monophopsphate (UMP) molecule for every UDP-GlcNAc molecule it introduces into Golgi.[40] The same occurs for all other transport proteins considered in this work.[41–43] These transport mechanisms have also been characterized quantitatively. In all cases, transport has been found to follow saturation kinetics, which depends on the concentration of the NSD on the cytosolic side of Golgi and on the respective dephosphorylated nucleotide concentration on the luminal side.[40–43] To generate a first link between cellular metabolism and N-linked glycosylation, the transport of NSDs has been added to our model. Using the information presented above, and considering that the interaction between transport substrates and the TP is analogous to enzyme–substrate interactions, the expression describing transport of NSDs into the Golgi apparatus is defined as Eq. 9. The derivation for this equation is presented in Supporting Information S2.

$$F_{k,\mathrm{in}} = k_{\mathrm{T},k}[\mathrm{TP}_k]\left(\frac{A_\mathrm{G}}{V_\mathrm{G}}\right)\left(\frac{[\mathrm{Pc}_k^{\mathrm{Cyt}}]}{K_{\mathrm{Pc}}^{\mathrm{Cyt}} + [\mathrm{Pc}_k^{\mathrm{Cyt}}]}\right)\left(\frac{[\mathrm{BP}_k^{\mathrm{G.L.}}]}{K_{\mathrm{BP}}^{\mathrm{G.L.}} + [\mathrm{BP}_k^{\mathrm{G.L.}}]}\right) \quad (9)$$

Parameter Values

Many of the parameters presented in this section are from different sources and different cell lines. Although this could limit confidence in the calculations, the parameters values have been selected to be the closest possible to the main mAb producing cell line (Chinese hamster ovary) and are the best available from literature. The overall cell volume considered in this work is 2,500 μm^3.[44] Combining this with structural information of the Golgi apparatus reported by Ladinsky et al.,[45] the volume of the Golgi apparatus was calculated as 25 μm^3. Assuming only four compartments and using an aspect ratio (diameter:thickness) of 60 to 1 (approximated from Ref. 45), the obtained internal diameter of the tube presented in Figure 2 is 7.82 μm. The overall length of the tube (length of the Golgi stack) is calculated as 0.52 μm. With this information, the surface area of a single compartment was calculated as 99 μm^2. We are aware that different cell lines have different Golgi sizes. The use of different Golgi dimensions would affect both our estimated length of the Golgi stack as well as the diameter of the Golgi space. However, for simulation purposes, the length of Golgi was normalized and hence has no impact on the material balances described in Eqs. 1–3.

The specific protein productivity was taken as 387 $\mathrm{pmol}(10^6\mathrm{cells})^{-1}\mathrm{day}^{-1}$.[46] This value falls within the range reported by Bibila and Robinson.[47] When considering that each mAb molecule contains two N-linked glycosylation sites, the glycan productivity for this system is 773 pmol $(10^6\mathrm{cells})^{-1}\mathrm{day}^{-1}$, which also lies within the range of 100 to 1,500 $\mathrm{pmol}(10^6\mathrm{cells})^{-1}\mathrm{day}^{-1}$ used in previous models.[17–19] Umaña and Bailey[19] estimated the residence time of proteins within the Golgi apparatus as 22 min, which seems reasonable considering that Hirschberg and Lippincott-Schwartz[48] reported an ER/Golgi residence time of 40 min with a protein flux equivalent to 574 $\mathrm{pmol}(10^6\mathrm{cells})^{-1}\mathrm{day}^{-1}$. The volumetric flowrate (q) through the Golgi space was defined as 1.12 $\mu m^3\ \mathrm{min}^{-1}$ and the concentration of glycoprotein that is transferred from the ER to the Golgi apparatus (i.e., the concentration of glycoprotein at $z = 0$) was defined as 600 μM. The ensuing concentration of mAb Fc glycans entering the Golgi apparatus is 1,200 μM. The kinetic and NSD transport parameters are presented in Tables 2–4. Details for the derivation of these parameters are presented in Supporting Information S3.

Parameter Estimation and Model Simulation

Parameter estimation for enzyme concentration profiles

The localization of the enzymes along the length of the Golgi (z), which is represented by the parameters $z_{j,\max}$ and $z_{k,\max}$ in Eqs. 4 and 5 were defined based on the experimental findings by Rabouille et al.[26] This group determined the distribution of ManII, GnTI, GalT, and SiaT by immunolabeling cryosections of HeLa cells, but left the distribution of GnTII and FucT unknown. This methodology generated a series of "snap-shots" of enzyme distribution related to the static compartment model of Golgi. The mathematical model presented herein attempts to describe the dynamics of Golgi cisternal maturation, for this reason, the data presented by Rabouille et al.[26] were further detailed by an optimization-based approach.

The parameters that define enzyme distribution were estimated by seeking the minimum amount of total enzyme (the integral of enzyme concentration over the length of Golgi) necessary to achieve terminal oligosaccharide processing, including 50% sialylation. The parameter values were obtained through a multiple-shooting control vector parametrization algorithm, which (i) choses the duration of each control interval and the values of the control and differential variables at the start of each control interval, (ii) solves the dynamic model over the time horizon to determine the time variation of all variables in the system and with them, obtains the values for the objective function, the constraints and the differences between computed values and the ones chosen by the optimizer at the start of each interval. (iii) The optimizer finally revises the first step and repeats the procedure until the objective function is minimized, the constraints are satisfied and the differential variables are continuous at the beginning of each control interval.[66] The calculated enzyme concentration profiles along with the estimated parameters that define them are presented in panel A of Figure 3. The enzymes appear in a sequential fashion but overlap considerably which is consistent with previous findings.[23,26] The order in which the enzymes appear is related to the reaction sequence itself. For example, the early mannose-trimming reactions occur at early stages of the reaction scheme, thus ManI appears first. Co-localization of enzymes was found to have an impact on the reaction kinetics (data not shown). Specifically, in simulations where ManI did not overlap with GnTI, higher overall enzyme concentration was necessary to achieve full removal of the mannose residues from the precursor oligosaccharide (GnTI pushes the mannose trimming reactions forward and, to an extent, avoids product inhibition of ManI activity). Similar effects were observed relating FucT with GnTII and GalT with SiaT. The total concentration of enzymes (the integral of the presented profiles over the length of Golgi, z) ranged between 3.2 μM and 9.1 μM, which is consistent with the glycosylation enzyme concentration range of 1 μM–35 μM estimated through multiplying the membrane-bound protein content of 38,000 protein molecules/μm^2 reported by Quinn et al.[67] by the molar fraction of Golgi glycosylation enzymes reported by Gilchrist et al.[68]

Table 2. Enzyme Kinetic Parameters

Enzyme turnover rates				
Enzyme	V_{max} (μmol mg^{-1} min^{-1})	Organisms	MW (g/mol)	k_f (min^{-1})
ManI	3.677	Human, purified[49]	230,000[50]	888
ManII	6.75	Rat liver, purified[28]	285,000[28]	1,924
GnTI	19.80	Rabbit liver, purified[51]	51,600[52]	1,022
GnTII	27.50	Rat liver, purified[31]	200,000[31]	1,406
GnTIII	5.52	Rat liver, purified[53]	114,000[53]	629
FucT	4.37	Porcine brain, purified[54]	66,530[54]	291
GalT	19.80	Rat liver, purified[55]	44,040[56]	872
SiaT	8.20	Rat, purified[57]	59,930[58]	491

Enzyme dissociation constants				
Enzyme	Substrate	K_i (μM)	K_k (μM)	Notes and References
ManI	Man_9	60.5	———	Estimated[27]
	Man_8	110.0	———	Human, purified[49]
	Man_7	30.8	———	Estimated[27]
	Man_6	74.1	———	Estimated[27]
ManII	Man_5	200.0	———	Purified human adenocarcinoma[59]
	Man_4	100.0	———	Estimated[18]
FucT	$CoreGlcNAc_2$	25.0	46.0	Porcine brain, purified[54]
	α-1,6 arm occupied	1.2		Estimated[18]
GnTI	Man_5	260.0	170.0	CHO, purified[60]
GnTII	$CoreGlcNAc_1$	190.0	960.0	Rat liver, purified[31]
GnTIII	$CoreGlcNAc_2$	21.0	420.0	Rat GnTIII expressed in insect cells[34]
GalT	$CoreGlcNAc_2$ (α-1,3 arm)	430.0		
	$CoreGlcNAc_2$ (α-1,6 arm)	130.0	65.0	Rat liver, purified[61]
	$CoreGlcNAc_2Gal_1$(α-1,6 arm)	6,280.0		
SiaT	Asialo glycoprotein	330.0	50.0	Rat expressed in COS-1 cells[62]

Table 3. Transport Kinetic Parameters

Transport protein	V_{max} (pmol mg$^{-1}_{prot}$ min^{-1})	$k_{T,k}$ (min^{-1})	$K^{Cyt}_{Pc,k}$ (μM)
TP_1 (UDP-GlcNAc/UMP)	915.0[40]	1,084	7.13[40]
TP_2 (GDP-Fuc/GMP)	1.4[43]	130.0	7.5[43]
TP_3 (UDP-Gal/UMP)	22.0[42]	689.0	2.4[42]
TP_4 (CMP-Neu5Ac/CMP)	335.0[41]	397.0	1.3[41]

Table 4. Nucleotide Sugar Concentration in Golgi Lumen and Cytosol

NSD	Total Intracellular Concentration (μM)	Concentration in Golgi Lumen (μM)	Concentration in Cytosol (μM)
UDP-GlcNAc	36.7[63]	1,057	26.4
GDP-Fuc	20.0[64]	576	14.4
UDP-Gal	9.2[63]	265	6.6
CMP-Neu5Ac	33.0[65]	950	23.7

A comparison between the estimated enzyme parameters and those reported by Rabouille et al.[26] are presented in panels B and C of Figure 3. The deviation between both sets of data is likely due to the underlying assumptions of the model: symmetric enzyme concentration profiles and minimum enzyme required for full oligosaccharide processing, but also because of the snap-shot representation of the Rabouille et al[26] data. The enzyme profiles presented in Figure 3 also satisfy previously reported properties: (i) GnTI co-localizes with ManII in the medial Golgi, (ii) GnTI, ManII, GalT, and SiaT coexist in the trans Golgi region, and (iii) GalT and SiaT co-localize in the trans Golgi (TG) and the TG network regions.[23,26] Hence, it is possible to consider the estimated enzyme concentration profiles as realistic.

Parameter estimation for transport protein concentration profiles

The transport protein concentration profiles were also assumed to follow normal functions so that the effect of Golgi resident protein recycling would be represented. Low availability of NSDs for the Golgi glycosylation reactions has been linked to cell metabolism and not to their defficient transport into the Golgi,[36–68] with the exception of Rijcken et al.,[69] who described an interesting control mechanism by which UDP-GlcNAc determines the transport of CMP-Neu5Ac into Golgi. This implies that when NSDs are sufficiently available in the cytosol, the transport of NSDs into the Golgi is very close to the rate of accumulation of respective by-products which, in turn, is the rate of consumption for each NSD. By assuming that the rate of by-product dephosphorylation is much faster than NSD accumulation, Eq. 10 was defined as the objective function and was minimized using a multiple-shooting control vector parameterization algorithm[66] to estimate the missing TP parameters.

$$OF_k = \int_0^1 \left(F_{k,in} - V \sum_{k=1}^{N.R} r_k \right)^2 dz \qquad (10)$$

A comparison between the rate of consumption of NSDs and the rate of their transport is provided in Supporting Information to this article (S4), where both sets of data overlap showing minimization of Eq. 10. Results for the parameter estimation are presented in panel D of Figure 3. It has been previously reported that the UDP-GlcNac TP closely co-localizes with ManII,[70] the UDP-Gal transporter with GalT,[71] and the CMP-Neu5Ac transporter with SiaT.[72] Comparing panel D with panel A of Figure 3 shows that these observations are satisfied. In addition, the estimated cumulative concentration of transport proteins along the Golgi apparatus ranges between 900 and 1,700 μmol/m^2 which is well within the total membrane-bound protein density of 38,000 protein molecules/μm^2 reported for the Golgi apparatus of baby hamster kidney cells.[67]

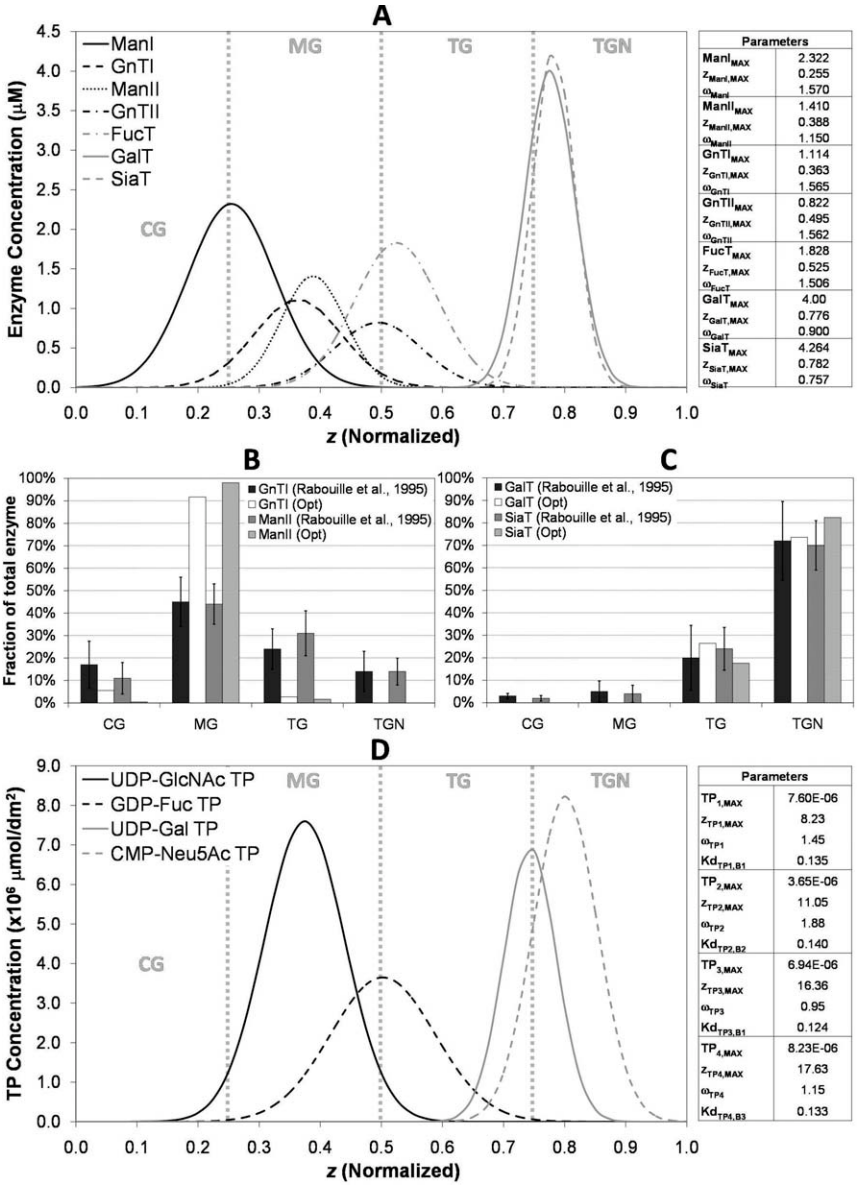

Figure 3. Resident protein profiles along the Golgi apparatus.

A: Calculated glycosylation enzyme concentration profiles. B and C: Compare the simulation results for enzyme distribution (patterned bars) with those previously reported by Rabouille et al.[26] (solid bars). D: Calculated TP concentration profiles. The light vertical lines in (A) and (D) present the regions of the Golgi apparatus. The tables alongside panels A and D present the parameters that were estimated to obtain the respective profiles.

Kinetic Parameter Estimation and Model Simulation

Most of the enzyme kinetic parameters were obtained through experiments performed using free oligosaccharides as substrates (see Table 2). However, Tabas and Kornfeld[27] also performed kinetic experiments using an immunoglobulin M-derived glycopeptide. Their results showed that at low glycopeptide concentrations, the kinetic parameters are similar to those of the free oligosaccharide, but at high glycopeptide concentration, the rates diverge, implying a change in affinity of the enzyme for the substrate. This evident change in enzyme–glycoprotein affinity along with the spatial constraints associated to the mAb Fc oligosaccharides served as the basis to consider the dissociation constants as the adjustment criterion when trying to match experimentally obtained mAb Fc oligosaccharide profiles.

Two recent publications reporting the oligosaccharide profiles of commercial mAbs[73,74] were used as target data so that unknown kinetic parameters of the model could be estimated. The data were introduced into the parameter estimation function of gPROMS version 3.3.1. The estimation algorithm uses the maximum likelihood formulation that attempts to determine values for the uncertain physical and variance model parameters which maximize the probability that the model will predict the values obtained from measurements.[66]

Parameter estimation was only performed for the dissociation constants of GnTII, FucT, and GalT because very low proportion of high mannose, hybrid, bisecting GlcNAc or sialylation were reported by Stadlmann et al.[74] or Nakano et al.[73] The $K_{d,i}$ for GnTIII and SiaT were defined as 1×10^{12} to represent that the oligosaccharide structures of the mAb Fc are inaccessible for GnTIII and SiaT. Also, the dissociation constant for the addition of galactose to the α-1,6 arm of the biantennary oligosaccharide when the α-1,3 arm

Table 5. Estimated Parameters and Deviations from Experimental Data

Dissociation constant (μM)	Herceptin	Rituxan	Remicade	Erbitux
$K_{d,i}^{GnTII}$	1,572	1,180	462	366
$K_{d,i}^{FucTA}$	711	593	176	145
$K_{d,i}^{FucTB}$	467	465	169	72
$K_{d,i}^{GalTa1A}$	143	166	24	5.4
$K_{d,i}^{GalTa1B}$	23	105	29	24
$K_{d,i}^{GalTa2A}$	59	87	149	510
Deviation from experimental data (%)	1.9	10.4	0.5	2.2

is already occupied ($K_{d,i}^{GalTa2B}$) was defined as 50-fold that of $K_{d,i}^{GalTa1A}$ based on the previously reported branch specificity of GalT.[61] The estimated parameters are presented in Table 5 and the terminal oligosaccharide profiles calculated with the estimated parameters are presented in Figure 4. Additional dynamic results showing the oligosaccharide profile distributions along the length of the Golgi apparatus (z) are presented in Supporting Information S5.

In Table 5, we see that the parameters estimated for the Nakano et al. data (Herceptin and Rituxan) fall within a narrow range. The same occurs for the parameters estimated for the Stadlmann et al. data. However, when comparing both parameter sets, there is larger variation. It is possible that these differences occur because the Nakano et al. data reports two oligosaccharide species more than the Stadlmann et al. does. It is likely that additional glycan data would yield more accurate estimates. The values for the estimated parameters do not diverge excessively from those presented in Table 2. It is possible that the differences can be attributed to the fact that the original values from Table 2 were obtained for enzymes that were purified from different cell types using free oligosaccharide species as substrates. We therefore believe that the obtained parameters are reasonable.

In three cases, the experimental data is reproduced to within 2.5% total deviation. The exception is Rituxan, where the net deviation is 10%. The main source for the larger deviation is the bi-galactosylated, core fucosylated oligosaccharide 57 shown in Figure 4. Three of the six dissociation constants that were estimated correspond to the specificity of GalT for different arms of the oligosaccharide. We believe that the higher deviation associated with OS_{57} in the Rituxan data is due to the constraints generated by the relationship between the three GalT dissociation constants. If the values for any of the $K_{d,i}^{GalT}$ parameters change, they affect the synthesis of more processed oligosaccharides and yield higher deviations associated to species OS_{31} and $OS_{44/45}$. In reality, each oligosaccharide species should have its own affinity for the different enzymes due to enzyme-substrate specificity. We believe that, for the Rituxan data, a deviation of 10% is acceptable considering that the number of GalT-associated $K_{d,i}$ parameters has been reduced from a maximum of 36 given by our reaction scheme (see Figure 1) to only three.

To our knowledge, this is the first report of such good agreement between model simulation results and experimentally obtained terminal glycosylation structures for commercial mAbs. We must mention that the experimental oligosaccharide profiles reported in Refs. 73,74 lack deviations and are therefore insufficient for generating confidence intervals for the estimated parameters. Additional experimental data, which must include variance and would ideally be dynamic in nature (time-course oligosaccharide profiles over a batch or fed-batch culture) are necessary to estimate the kinetic parameters more accurately and associate confidence intervals to them.

Comparison with Previous Models

Effect of kinetic mechanisms

As mentioned in previous sections, the present model builds on the knowledge generated by previous models of the Golgi N-linked glycosylation process. In the three previous models,[17–19] all enzymes involved in the sugar addition reactions of the process were assumed to act with a random-order kinetic mechanism. However, literature suggests that GnTI, GnTII, and GalT function with a sequential-order kinetic mechanism.[31,32] When comparing the rate expressions derived for both mechanisms, we find that there are additional terms in the denominator for the random-order kinetic expression (see the denominator of Eqs. 6 and 7). These terms correspond to additional enzyme–substrate complexes (EOS_i, EOS_z, and EOS_{i+1}) that occur in random-order kinetics but are absent in sequential-order kinetics.

Figure 5 compares the kinetic mechanisms assumed by previous models (only random-order) with the mechanisms we have derived in this work (combination of sequential-order and random-order kinetics, see Table 1). Figure 5A compares the impact the different mechanisms have on the reaction rate values, and Figure 5B shows how considering the appropriate kinetic mechanisms influence the oligosaccharide profiles calculated by the model. From the data, it is clear that the different kinetic mechanisms indeed affect the calculated oligosaccharide profiles. To assess the impact of the different kinetic mechanisms on parameter estimation, the dissociation constants for the mAb-bound oligosaccharides were estimated as described in the previous section but with the model containing only random-order kinetics. Successful reproduction of the commercial mAb oligosaccharide profiles was achieved (data not shown). However, we believe that including the actual kinetic mechanisms for each enzyme generates no further complexity in the model, and therefore, should be used to represent the Golgi glycosylation process with higher realism.

Model performance and parameter estimation strategy

The only previous model that attempted to reproduce experimentally observed oligosaccharide profiles was that of Krambeck and Betenbaugh.[18] They attempted to match the oligosaccharide profiles for human thrombopoietin by adjusting the total glycosylation enzyme concentration while maintaining the corresponding spatial distributions constant. In contrast, Hossler et al.[17] did not try to match experimental data given the scope of their work. Instead, they estimated the glycosylation enzyme concentrations that would maximize terminally processed oligosaccharides. Under this methodology, Hossler et al. also assumed enzyme distribution along Golgi as constant.

To compare the performance of our model with the previous ones, we defined each of them, including their underlying assumptions and parameters in gPROMS 3.3.1. The sole modification was that the reaction scheme was reduced to the one presented in Figure 1, which is specific for mAb Fc

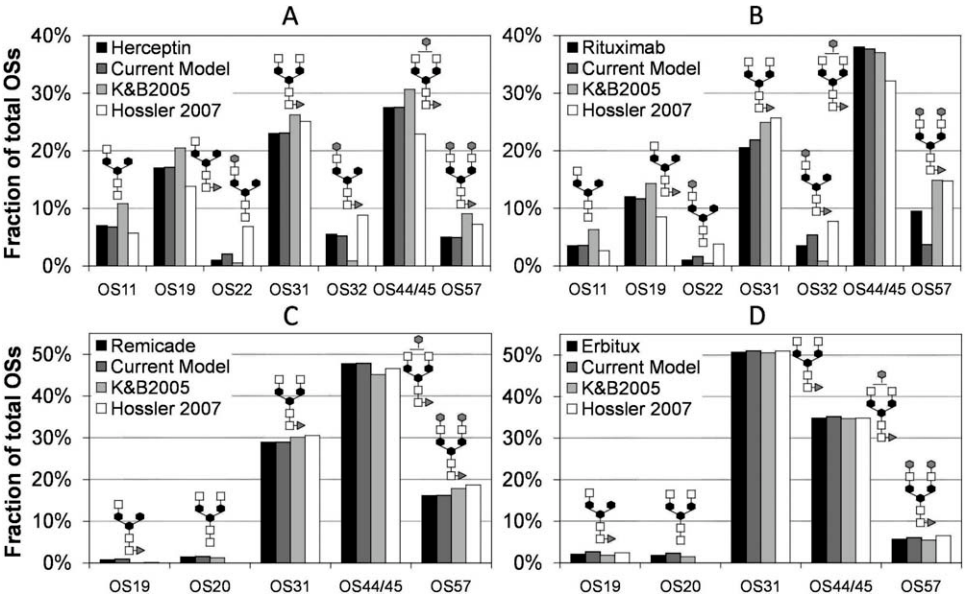

Figure 4. Calculated vs. experimental oligosaccharide profiles.

The dark bars correspond to the experimental oligosaccharide profiles, and the dark gray bars represent those calculated with the current model. The light gray bars show the profiles calculated with Krambeck and Betenbaugh's model and the white bars present those calculated with the Hossler et al. model. Comparison between Herceptin (A), Rituxan (B), Remicade (C), and Erbitux (D) are shown. Experimental data for A and B were obtained from Nakano et al.[73] and for (C) and (D) was obtained from Stadlmann et al.[74] Tables 5 and 6 present the estimated parameters with which all profiles were calculated.

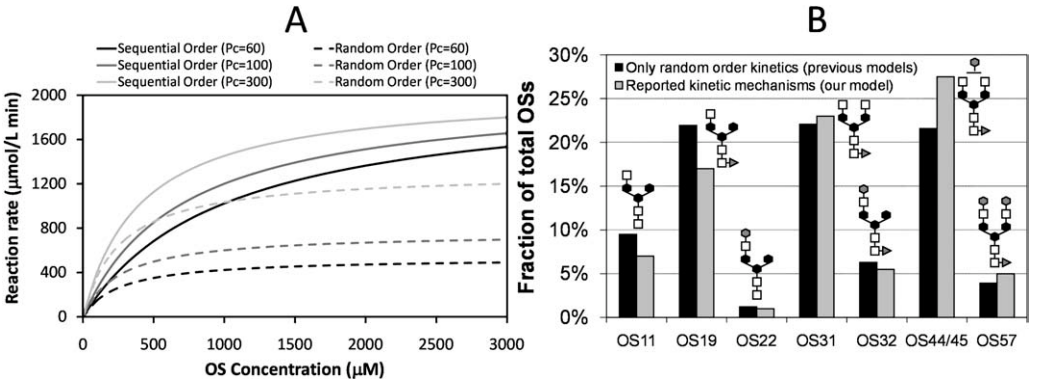

Figure 5. Comparison with previous models.

A: Compares the profiles of sequential-order kinetics (solid lines) and random-order kinetics (dashed line) with respect to oligosaccharide concentration at three different donor concentrations (60, 100, and 300 mM). B: Compares the calculated oligosaccharide profiles with only random-order kinetics (dark bars) to those calculated with the actual mechanism for each enzyme (light bars).

oligosaccharides. When simulating both models with their original parameters, they both calculated unrealistically high proportions of the bi-galactosylated and core fucosylated oligosaccharide 57 (76% for Krambeck and Betenbaugh and 41% for Hossler et al). These values are five and 2.5 times the value of 16.1% reported for Remicade presented in Figure 4. The large discrepancies are likely due to the combination of parameters and assumptions the previous authors considered and make the results uncomparable with those generated by our model.

So that a more reasonable comparison between the different models is produced, we used the strategy proposed by Krambeck and Betenbaugh for estimating the total enzyme concentration to match experimental oligosaccharide profiles. To ensure comparability, the same number of parameters were estimated in all cases: six dissociation constants for the current model (as described in the previous section) and the total concentration of six glycosylation enzymes for the previous models. This approach was implemented in the parameter estimation function of gPROMS version 3.3.1 which has been described in previous sections of this article. The estimated parameters, along with the deviations from the experimental data are presented in Table 6.

It is clear from the data presented in Table 6 that the values obtained for both of the previous models is dissimilar. This is very likely due to differences in the kinetic parameters assumed by each model. Namely, Hossler and collaborators derived the turnover rate for each enzyme by multiplying the reported maximum reaction rate by the molecular weight of the monomeric form of each enzyme, while Krambeck and Betenbaugh assumed the molecular weight to be that of the entire enzymatic complex. Because of this, the estimated enzyme concentrations for the Hossler et al. model are much higher than those estimated for the Krambeck and

Table 6. Estimated Parameters with Previous Models

	Estimated Values							
	K&B Model (μM)				Hossler Model (μM)			
Enzyme	Herceptin	Rituxan	Remicade	Erbitux	Herceptin	Rituxan	Remicade	Erbitux
ManI	1.21	1.50	1.67	2.06	20.85	19.91	27.34	27.95
ManII	9.29	6.16	4.07	1.77	6.20	21.88	6.97	9.22
GnTI	2.54	1.58	9.27	3.98	7.72	9.58	2.35	2.40
GnTII	0.18	0.23	1.58	0.36	0.30	0.49	0.64	0.42
FucT	0.82	0.85	0.82	0.81	1.10	1.59	18.89	17.15
GalT	0.014	0.019	0.021	0.012	8.18	10.62	10.46	6.34
Deviation from experimental data (%)	22.9	19.0	6.4	0.9	22.6	27.7	7.4	3.3

Betenbaugh model. It is worth noting that due to this assumption by Hossler et al., the total amount of resident protein (both with the original enzyme concentrations and the estimated ones), present in the Golgi is much higher than the maximum membrane bound protein density reported by Quinn et al.,[67] thus deeming these concentration profiles unfeasible. In contrast, in the current model, the total amount of resident protein in Golgi is approximately 60% of the value reported by Quinn et al.[67] This, along with the implication of resident protein recycling from the Golgi maturation model, suggests that our estimated resident protein profiles are more realistic than simple constant concentration profiles for resident proteins.

A comparison of the terminal oligosaccharide profiles calculated with the estimated parameters has been included in Figure 4. All but one case (Erbitux profiles calculated with the Krambeck and Betenbaugh model) show much larger deviations from the experimental data than those obtained with our proposed model and parameter estimation strategy. On average, our strategy of estimating dissociation constants yields deviations which are 4.5 times lower than those obtained with the Krambeck and Betenbaugh model and 5.5 times lower than those obtained with the Hossler et al. model. The cause of these discrepancies are a combination of model structure and the estimation strategy itself (estimating $K_{d,i}$s vs. estimating enzyme concentrations).

To isolate these effects, a second series of parameter estimations were performed on the previous models. In this case, the enzyme concentrations were set at the original values assumed by each model and the dissociation constants were estimated. When estimated for the Krambeck and Betenbaugh model, the $K_{d,i}$s produced terminal oligosaccharide profiles that deviate five times more than the current model. The results for the Hossler et al. $K_{d,i}$ estimation deviated nine times more than those presented in Table 5. In both cases, the deviations are higher than those obtained by estimating total enzyme concentration. These results suggest that the reason why the current model outperforms the previous ones is due to structure and not the estimation strategy. More specifically, the results suggest that the definition of the glycosylation enzyme distributions is why the current model outperforms the previous ones in reproducing experimental oligosaccharide profiles. To confirm this, a final set of parameter estimations were performed to obtain the distribution of glycosylation enzymes that could match experimental data. In this case, the estimations yielded results that are comparable with those obtained with the model presented herein (data not shown). However, it is worth noting that, in these cases, 24 parameters were estimated: the concentration of the six glycosylation enzymes in each of the four Golgi compartments. It is likely that good reproduction of the experimental oligosaccharide profiles was achieved due to overfitting.

This section has compared the performance of the current model with previous ones. The results suggest that the present model along with the methods used to estimate its unknown parameters outperforms the previous ones in reproducing experimental mAb Fc oligosaccharide profiles. Furthermore, if mathematical models for mAb Fc N-linked glycosylation were to be used for bioprocess design, control, and optimization following the QbD paradigm, it would be necessary for them to represent all the relevant known phenomena surrounding the process. In this section, we have shown that our additional considerations (appropriate kinetic mechanisms and Golgi protein recycling) have contributed to the fidelity of the model while avoiding significant additional complexity.

Case Studies

Case study 1: gene silencing simulations

Additional simulations were performed to further assess the performance of the model against independet sets of data. These simulations were based on the study by Imai-Nishiya et al.,[75] in which the gene encoding for the FucT enzyme was silenced using small interfering RNA. As a first step, the dissociation constants for GnTII, FucT, and GalT were estimated (as described in preceding sections) to match the parental oligosaccharide profile. A comparison between the calculated and parental oligosaccharide profiles is presented as panel A of Figure 6, which shows that the profiles obtained through simulation closely match the reported ones yielding a net deviation of 3.4%. Next, the concentration of FucT was set to zero within the model and a simulation was performed. A comparison of the simulated and reported oligosaccharide profiles after FucT silencing is presented in panel B of Figure 6. In this case, a slightly higher deviation of 4.7% was obtained. The same procedure was performed with the Krambeck and Betenbaugh and the Hossler et al. model. The Hossler et al. model had a net deviation of 4.0%, which is comparable with the one obtained with the current model. In contrast, the Krambeck and Betenbaugh model had a deviation of 17%. On setting the FucT concentration to zero, the Hossler et al. model calculated oligosaccharide distributions with a 19.3% deviation from the experimental ones, while the Krambeck and Betenbaugh model had a 20% deviation. These results show that the current model is capable of reproducing the effect of genetic silencing of a glycosylation enzyme to a very high degree whereas the previous models seem incapable of reproducing the effect accurately. The fact that the current

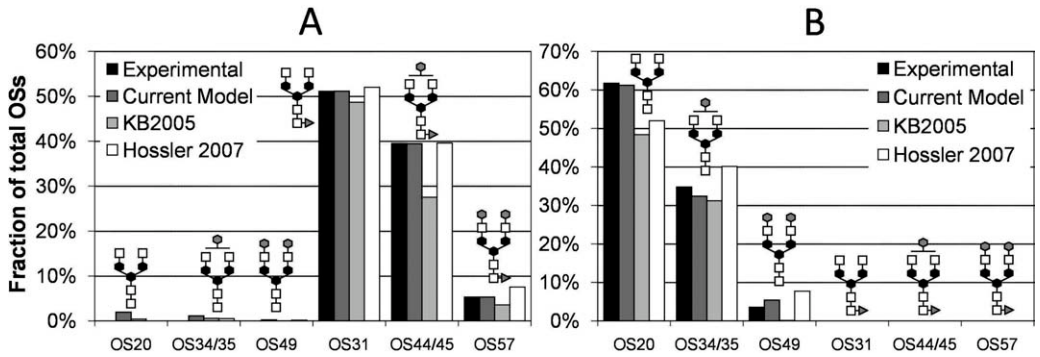

Figure 6. FucT silencing.

A: Compares the reported oligosaccharide profiles (dark bars) with the ones calculated with the current model (dark gray bars), the Krambeck and Betenbaugh model (light gray bars), and the Hossler et al. model (white bars) before FucT gene silencing. B: Compares reported and calculated oligosaccharide profiles after FucT silencing. The reported data were obtained from Imai-Nishiya et al.[75]

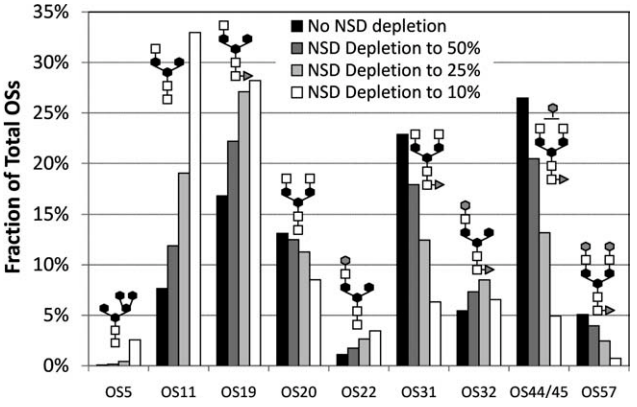

Figure 7. NSD depletion.

Calculated oligosaccharide profiles obtained when cytosolic NSD concentrations are constant (dark bars) and depleted to 50%, 25%, and 10% of their initial value (increasingly lighter bars, respectively).

model reproduces this phenomenon so effectively makes it useful for exploring cell engineering strategies for the production of mAbs with a desired oligosaccharide profile.

Case study 2: cytosolic NSD depletion

The final element that the present model includes is the transport of NSDs from the cytosol to the Golgi apparatus by means of transport proteins. The purpose of including the transport of these compounds into the Golgi apparatus is to link their concentrations with the glycosylation profiles of mAbs. Previous studies have shown that the concentration of NSDs vary throughout cell culture and that this affects the produced glycoform distribution.[38,76,77] As a means of demonstrating the capability our model has of representing this effect, simulations were performed where the concentration of NSDs in the cytosol decreased to 50%, 25%, and 10% of their initial value.

Figure 7 shows that with decreasing cytosolic NSD concentrations, the relative amount of less-processed oligosaccharides increases. This result is in agreement with previously reported data that associates NSD availability in the cytosol with shifts in oligosaccharide profiles to less-processed ones, including a considerable increases in high mannose and hybrid oligosaccharides.[38] This result is fairly intuitive: if availability of NSDs in the cytosol is limited, their rate of transport into the Golgi will be reduced, thus also limiting their availability in the Golgi lumen. In Figure 7, we show that our model indeed has the ability to link time-varying cytosolic NSD concentrations with oligosaccharide distributions. This connection with cellular metabolism should allow for the assessment of metabolic effects on Golgi N-linked glycosylation and provides a more detailed picture of how the N-linked glycosylation process occurs.

Conclusions

The model presented herein has approximated the Golgi apparatus as a single PFR to simulate mAb N-linked glycosylation in maturing Golgi cisternae. Model-based optimization methods have been developed to estimate parameters associated with resident protein concentration profiles along the length of the Golgi apparatus. These methods generate results that are in good agreement with previously reported observations. Additional optimization methods have been implemented for the estimation of enzyme kinetic parameters. With the obtained parameters, the model has been shown to closely represent experimentally determined oligosaccharide profiles of mAbs. The current model was compared with previous ones to assess the effect of its new considerations. We found that including the actual kinetic mechanisms produces results that are different from those obtained with previous model's kinetic expressions. We have also found that the model and its underlying assumptions are able to reproduce experimentally obtained mAb Fc oligosaccharide profiles with much higher accuracy than either of the previous models. Finally, many of the considerations that have been implemented in the current model add little complexity to the model, and where complexity has been added, it has been overcome by the optimization-based methodologies developed in this work.

We have demonstrated that the model accurately reproduces the effect of FucT silencing on mAb oligosaccharide profiles. This capability can prove useful for exploring cell engineering strategies to achieve mAbs with defined glycosylation profiles. In addition, we have shown that the model is able to represent the effect of decreasing NSD concentrations on the oligosaccharide profiles of the glycoprotein. When coupled to a model for NSD metabolism, a direct link will be generated between an extracellular (and measurable) quantity such as glucose concentration with glycosylation patterns of mAbs. Such a combined model could potentially be used for bioprocess design, control, and optimization.

The results presented herein are promising and further experimental work will help increase confidence in its predictive capability. Information surrounding the localization of Golgi resident proteins can be complemented by the use of in vivo protein imaging techniques such as those reviewed by Lippincott-Schwartz.[78] Detailed and time-dependent data on the oligosaccharide profiles of mAbs will also be useful to estimate model parameters with higher confidence.

Toward the future, the model presented herein can be used to identify process parameters that are crucial for accurate prediction of the glycoform distribution of mAbs and, by extension, of more complex glycoproteins. This, in turn, can be used to design experiments that promote understanding of N-linked glycosylation and thus, possibly facilitate the design, control, and optimization of therapeutic protein production processes under the QbD scope.

Acknowledgment

IJV wishes to thank the Mario Molina Fund and CONACYT for his scholarships. CK thanks Lonza Biologics for her fellowship.

Notation

OS_i = oligosaccharide chain i (acceptor)
Pc_k = nucleotide-sugar precursor k (donor)
B_k = by-product k. It is the nucleotide component of the NSDs (UDP, GDP, or CMP)
F_{in} = flowrate of oligosaccharide 1 into the Golgi cisterna
$F_{k,in}$ = flowrate of NSD k into the Golgi cisterna
q = volumetric flowrate into the Golgi cisterna
D_i = internal diameter of the Golgi space
$v_{i,j}$ = stoichiometric coefficient of oligosaccharide i in reaction j
$v_{k,j}$ = stoichiometric coefficient of NSD k in reaction j
r_j = rate of reaction j
$E_j(z)$ = concentration of enzyme j along Golgi length, z
$E_{j,max}$ = peak concentration of enzyme j
$z_{j,max}$ = localization of the peak concentration of enzyme j
ω_j = width of the concentration profile of enzyme j
$TP_k(z)$ = concentration of TP k along Golgi length, z
$TP_{k,max}(z)$ = peak concentration of TP k
$z_{k,max}(z)$ = localization of the peak concentration of TP k
ω_k = width of the concentration profile of TP k
k_f = rate-limiting turnover rate for reaction j
$K_{d,i}$ = dissociation constant of the acceptor–enzyme complex
OS_z = competing oligosaccharide substrates for the same enzyme (competitor)
$K_{d,z}$ = dissociation constant of the competitor–enzyme complex
OS_{i-1} = oligosaccharide product in the mannosidase reactions
$K_{d,k}$ = dissociation constant of the donor–enzyme complex
K_{d,B_k} = dissociation constant of the BP–enzyme complex
OS_{i+1} = oligosaccharide chain with additional sugar residue added (product)
$K_{d,i+1}$ = dissociation constant of the enzyme–product complex
$k_{T,k}$ = transport turnover rate
A_G = surface area of the Golgi cisterna
V_G = volume of the Golgi cisterna
Pc_k^{Cyt} = nucleotide-sugar precursor k concentration on the cytosolic side of Golgi
K_{Pc}^{Cyt} = dissociation constant of the transport protein–NSD complex
$BP_k^{G.L.}$ = by-product k in the Golgi lumen (same as B_k)
$K_{BP}^{G.L.}$ = dissociation constant of the transport protein–byproduct complex
ManI = α-1,2 mannosidase I
GnTI = α-1,3 *N*-acetylglucosaminyl transferase I
ManII = α-1,3/α-1,6 mannosidase II
GnTII = α-1,6 *N*-acetylglucosaminyl transferase II
FucT = α-1,6 fucosyltransferase (also known as FUT8)
GalT = β-1,4 galactosyltransferase
SiaT = α-1,6 sialyltransferase
TP_1 = transport protein for UDP-GlcNAc/UMP
TP_2 = transport protein for GDP-Fuc/GMP
TP_3 = transport protein for UDP-Gal/UMP
TP_4 = transport protein for CMP-Neu5Ac/CMP
COPI = Coat Protein Complex I
UDP = Uridine Diphosphate
GDP = Guanosine Diphosphate
CMP = Cytosine Monophosphate
UMP = Uridine Monophosphate
GMP = Guanosine Monophosphate

Literature Cited

1. Aggarwal S. What's fueling the biotech engine-2009–2010. *Nat Biotechnol*. 2010;28:1165–1171.
2. Jefferis R. Glycosylation as a strategy to improve antibody-based therapeutics. *Nat Rev Drug Discov*. 2009;8:226–234.
3. Chen X, Liu YD, Flynn GC. The effect of Fc glycan forms on human IgG2 antibody clearance in humans. *Glycobiology*. 2009;19:240–249.
4. Wright A, Morrison SL. Effect of C2-associated carbohydrate structure on Ig effector function: studies with chimeric mouse-human IgG1 antibodies in glycosylation mutants of Chinese hamster ovary cells. *J Immunol*. 1998;160:3393–3402.
5. Raju TS. Terminal sugars of Fc glycans influence antibody effector functions of IgGs *Curr Opini Immunol*. 2008;20:471–478.
6. Butler M. Optimisation of the cellular metabolism of glycosylation for recombinant proteins produced by Mammalian cell systems. *Cytotechnology*. 2006;50:57–76.
7. Hossler P, Khattak SF, Li ZJ. Optimal and consistent protein glycosylation in mammalian cell culture. *Glycobiology*. 2009;19:936–949.
8. Val IJ, Kontoravdi C, Nagy JM. Towards the implementation of quality by design to the production of therapeutic monoclonal antibodies with desired glycosylation patterns. *Biotechnol Prog*. 2010;26:1505–1527.
9. Rathore AS, Winkle H. Quality by design for biopharmaceuticals. *Nat Biotechnol*. 2009;27:26–34.
10. Rathore AS. Saleki-Gerhardt A,Montgomery SH.,Tyler SM. Quality by design: industrial case studies on defining and implementing design space for pharmaceutical processes Part 2. *BioPharm Int*. 2009;22:36–45.
11. Holland M, Yagi H, Takahashi N, Kato K, Savage COS, Goodall DM, Jefferis R. Differential glycosylation of polyclonal IgG, IgG-Fc and IgG-Fab isolated from the sera of patients with ANCA-associated systemic vasculitis *Biochim Biophys Acta-Gen Subjects*. 2006;1760:669–677.
12. Kornfeld R, Kornfeld S. Assembly of asparagine-linked oligosaccharides. *Annu Rev Biochem*. 1985;54:631–664.
13. Wormald MR, Rudd PM, Harvey DJ,Chang SC,Scragg IG,Dwek RA. Variations in oligosaccharide-protein interactions in immunoglobulin G determine the site-specific glycosylation profiles and modulate the dynamic motion of the Fc oligosaccharides. *Biochemistry*. 1997;36:1370–1380.
14. Flynn GC, Chen X, Liu YD, Shah B, Zhang Z. Naturally occurring glycan forms of human immunoglobulins G1 and G2. *Mol Immunol*. 2010;47:2074–2082.
15. Kobata A. The N-linked sugar chains of human immunoglobulin G: their unique pattern, and their functional roles. *Biochim Biophys Acta*. 2008;1780:472–478.
16. Shelikoff M, Sinskey AJ, Stephanopoulos G. A modeling framework for the study of protein glycosylation. *Biotechnol Bioeng*. 1996;50:73–90.
17. Hossler P, Mulukutla BC, Hu WS. Systems analysis of N-glycan processing in mammalian cells. *PLoS ONE*. 2007;2:e713.
18. Krambeck FJ, Betenbaugh MJ. A mathematical model of N-linked glycosylation. *Biotechnol Bioeng*. 2005;92:711–728.

19. Umaña P, Bailey JE. A mathematical model of N-linked glycoform biosynthesis. *Biotechnol Bioeng*. 1997;55:890–908.
20. Glick BS, Nakano A. Membrane traffic within the Golgi apparatus. *Annu Rev Cell Dev Biol*. 2009;25:113–132.
21. Losev E, Reinke CA, Jellen J, Strongin DE, Bevis BJ, Glick BS. Golgi maturation visualized in living yeast. *Nature*. 2006;441:1002–1006.
22. Matsuura-Tokita K, Takeuchi M, Ichihara A, Mikuriya K, Nakano A. Live imaging of yeast Golgi cisternal maturation. *Nature*. 2006;441:1007–1010.
23. Nilsson T, Au CE, Bergeron JJM. Sorting out glycosylation enzymes in the Golgi apparatus. *FEBS Lett*. 2009;583:3764–3769.
24. Glick BS, Malhotra V. The curious status of the Golgi apparatus. *Cell*. 1998;95:883–889.
25. Pelham HR. Getting through the Golgi complex. *Trends Cell Biol*. 1998;8:45–49.
26. Rabouille C, Hui N, Hunte F, et al. Mapping the distribution of Golgi enzymes involved in the construction of complex oligosaccharides. *J Cell Sci*. 1995;108 (pt 4):1617–1627.
27. Tabas I, Kornfeld S. Purification and characterization of a rat liver Golgi alpha-mannosidase capable of processing asparagine-linked oligosaccharides. *J Biol Chem*. 1979;254:11655–11663.
28. Moremen KW, Touster O, Robbins PW. Novel purification of the catalytic domain of Golgi alpha-mannosidase II. Characterization and comparison with the intact enzyme. *J Biol Chem*. 1991;266:16876–16885.
29. Velasco A, Hendricks L, Moremen KW, Tulsiani DR, Touster O, Farquhar MG. Cell type-dependent variations in the subcellular distribution of alpha-mannosidase I and II. *J Cell Biol*. 1993;122:39–51.
30. Unligil UM, Zhou S, Yuwaraj S, Sarkar M, Schachter H, Rini JM. X-ray crystal structure of rabbit N-acetylglucosaminyltransferase I. Catalytic mechanism and a new protein superfamily. *EMBO J*. 2000;19:5269–5280.
31. Bendiak B, Schachter H. Control of glycoprotein synthesis. Kinetic mechanism, substrate specificity, and inhibition characteristics of UDP-*N*-acetylglucosamine:alpha-D-mannoside beta 1–2 N-acetylglucosaminyltransferase II from rat liver. *J Biol Chem*. 1987;262:5784–5790.
32. Ramakrishnan B, Boeggeman E, Ramasamy V, Qasba PK. Structure and catalytic cycle of beta-1,4-galactosyltransferase. *Curr Opin Struct Biol*. 2004;14:593–600.
33. Ihara H, Ikeda Y, Toma S, Wang X, Suzuki T, Gu J, Miyoshi E, Tsukihara T, Honke K, Matsumoto A, Nakagawa A, Taniguchi N. Crystal structure of mammalian alpha1,6-fucosyltransferase, FUT8. *Glycobiology*. 2007;17:455–466.
34. Ikeda Y, Koyota S, Ihara H, Yamaguchi Y, Korekane H, Tsuda T, Sasai K, Taniguchi N. Kinetic basis for the donor nucleotide-sugar specificity of beta1, 4-*N*-acetylglucosaminyltransferase III. *J Biochem*. 2000;128:609–619.
35. Bendiak B, Cook GM. Kinetic parameters of a beta-*D*-galactoside alpha 2 leads to 6 sialyltransferase from embryonic chicken liver. *Eur J Biochem*. 1982;128:355–362.
36. Baker KN, Rendall MH, Hills AE, Hoare M, Freedman RB, James DC. Metabolic control of recombinant protein N-glycan processing in NS0 and CHO cells. *Biotechnol Bioeng*. 2001;73:188–202.
37. Nyberg GB, Balcarcel RR, Follstad BD, Stephanopoulos G, Wang DIC. Metabolic effects on recombinant interferon-gamma glycosylation in continuous culture of Chinese hamster ovary cells. *Biotechnol Bioeng*. 1999;62:336–347.
38. Wong DCF, Wong KTK, Goh LT, Heng CK, Yap MGS. Impact of dynamic online fed-batch strategies on metabolism, productivity and N-glycosylation quality in CHO cell cultures. *Biotechnol Bioeng*. 2005;89:164–177.
39. Hirschberg CB, Robbins PW, Abeijon C. Transporters of nucleotide sugars, ATP, and nucleotide sulfate in the endoplasmic reticulum and Golgi apparatus. *Annu Rev Biochem*. 1998;67:49–69.
40. Waldman BC, Rudnick G. UDP-GlcNAc transport across the Golgi membrane: electroneutral exchange for dianionic UMP. *Biochemistry*. 1990;29:44–52.
41. Lepers A, Shaw L, Cacan R, Schauer R, Montreuil J, Verbert A. Transport of CMP-N-glycoloylneuraminic acid into mouse liver Golgi vesicles. *FEBS Lett*. 1989;250:245–250.
42. Milla ME, Clairmont CA, Hirschberg CB. Reconstitution into proteoliposomes and partial purification of the Golgi apparatus membrane UDP-galactose, UDP-xylose, and UDP-glucuronic acid transport activities. *J Biol Chem*. 1992;267:103–107.
43. Sommers LW, Hirschberg CB. Transport of sugar nucleotides into rat liver Golgi. A new Golgi marker activity. *J Biol Chem*. 1982;257:10811–10817.
44. Frame KK, Hu WS. Cell volume measurement as an estimation of mammalian cell biomass. *Biotechnol Bioeng*. 1990;36:191–197.
45. Ladinsky MS, Mastronarde DN, McIntosh JR, Howell KE, Staehelin LA. Golgi structure in three dimensions: functional insights from the normal rat kidney cell. *J Cell Biol*. 1999;144:1135–1149.
46. Kontoravdi C, Pistikopoulos EN, Mantalaris A. Systematic development of predictive mathematical models for animal cell cultures. *Comput Chem Eng*. 2010;34:1192–1198.
47. Bibila TA, Robinson DK. In pursuit of the optimal fed-batch process for monoclonal antibody production. *Biotechnol Prog*. 1995;11:1–13.
48. Hirschberg K, Lippincott-Schwartz J. Secretory pathway kinetics and in vivo analysis of protein traffic from the Golgi complex to the cell surface. *FASEB J*. 1999;13 (suppl 2):S251–S256.
49. Karaveg K, Moremen KW. Energetics of substrate binding and catalysis by class 1 (glycosylhydrolase family 47) alpha-mannosidases involved in N-glycan processing and endoplasmic reticulum quality control. *J Biol Chem*. 2005;280:29837–29848.
50. Tulsiani DR, Touster O. Mannosidase IA from rat liver Golgi membranes. *Methods Enzymol*. 1989;179:446–451.
51. Nishikawa Y, Pegg W, Paulsen H, Schachter H. Control of glycoprotein synthesis. Purification and characterization of rabbit liver UDP-N-acetylglucosamine:alpha-3-D-mannoside beta-1,2-N-acetylglucosaminyltransferase I. *J Biol Chem*. 1988;263:8270–8281.
52. Fukada T, Iida K, Kioka N, Sakai H, Komano T. Cloning of a cDNA encoding N-acetylglucosaminyltransferase I from rat liver and analysis of its expression in rat tissues. *Biosci Biotechnol Biochem*. 1994;58:200–201.
53. Nishikawa A, Ihara Y, Hatakeyama M, Kangawa K, Taniguchi N. Purification, cDNA cloning, and expression of UDP-N-acetylglucosamine: beta-D-mannoside beta-1,4N-acetylglucosaminyltransferase III from rat kidney. *J Biol Chem*. 1992;267:18199–18204.
54. Uozumi N, Yanagidani S, Miyoshi E, Ihara Y, Sakuma T, Gao CX, Teshima T, Fujii S, Shiba T, Taniguchi N. Purification and cDNA cloning of porcine brain GDP-L-Fuc:N-acetyl-beta-D-glucosaminide alpha1–>6fucosyltransferase. *J Biol Chem*. 1996;271:27810–27817.
55. Bendiak B, Ward LD, Simpson RJ. Proteins of the Golgi apparatus. Purification to homogeneity, N-terminal sequence, and unusually large Stokes radius of the membrane-bound form of UDP-galactose:N-acetylglucosamine beta 1–4galactosyltransferase from rat liver. *Eur J Biochem*. 1993;216:405–417.
56. Gerhard DS, Wagner L, Feingold EA, Shenmen CM, Grouse LH, Schuler G, Klein SL, Old S, Rasooly R, Good P, Guyer M, Peck AM, Derge JG, Lipman D, Collins FS, Jang W, Sherry S, Feolo M, Misquitta L, Lee E, Rotmistrovsky K, Greenhut SF, Schaefer CF, Buetow K, Bonner TI, Haussler D, Kent J, Kiekhaus M, Furey T, Brent M, Prange C, Schreiber K, Shapiro N, Bhat NK, Hopkins RF, Hsie F, Driscoll T, Soares MB, Casavant TL, Scheetz TE, stein MJB, Usdin TB, Toshiyuki S, Carninci P, Piao Y, Dudekula DB, Ko MSH, Kawakami K, Suzuki Y, Sugano S, Gruber CE, Smith MR, Simmons B, Moore T, Waterman R, Johnson SL, Ruan Y, Wei CL, Mathavan S, Gunaratne PH, Wu J, Garcia AM, Hulyk SW, Fuh E, Yuan Y, Sneed A, Kowis C, Hodgson A, Muzny DM, McPherson J, Gibbs RA, Fahey J, Helton E, Ketteman M, Madan A, Rodrigues S, Sanchez A, Whiting M, Madari A, Young AC, Wetherby KD, Granite SJ, Kwong PN, Brinkley CP, Pearson RL, Bouffard GG, Blakesly RW, Green ED, Dickson MC, Rodriguez AC, Grimwood J, Schmutz J, Myers RM, Butterfield YSN, Griffith M, Griffith OL, Krzywinski MI, Liao N, Morin R, Morrin R, Palmquist D, Petrescu AS, Skalska U, Smailus DE, Stott JM, Schnerch A, Schein JE, Jones SJM, Holt RA,

Baross A, Marra MA, Clifton S, Makowski KA, Bosak S, Malek J. The status, quality, and expansion of the NIH full-length cDNA project: the Mammalian Gene Collection (MGC). *Genome Res*. 2004;14:2121–2127.
57. Weinstein J, Silva U, Paulson JC. Purification of a Gal beta 1 to 4GlcNAc alpha 2 to 6 sialyltransferase and a Gal beta 1 to 3(4)GlcNAc alpha 2 to 3 sialyltransferase to homogeneity from rat liver. *J Biol Chem*. 1982;257:13835–13844.
58. Harduin-Lepers A, Mollicone R, Delannoy P, Oriol R. The animal sialyltransferases and sialyltransferase-related genes: a phylogenetic approach. *Glycobiology*. 2005;15:805–817.
59. Chandrasekaran EV, Davila M, Nixon D, Mendicino J. Purification and properties of alpha-D-mannose:beta-1,2-N-acetylglucosaminyl-transferases and alpha-D-mannosidases from human adenocarcinoma. *Cancer Res*. 1984;44:4059–4068.
60. Chen W, Unligil UM, Rini JM, Stanley P. Independent Lec1A CHO glycosylation mutants arise from point mutations in N-acetylglucosaminyltransferase I that reduce affinity for both substrates. Molecular consequences based on the crystal structure of GlcNAc-TI. *Biochemistry*. 2001;40:8765–8772.
61. PÃćquet MR, Narasimhan S, Schachter H, Moscarello MA. Branch specificity of purified rat liver Golgi UDP-galactose: N-acetylglucosamine beta-1,4-galactosyltransferase. Preferential transfer of of galactose on the GlcNAc beta 1,2-Man alpha 1,3-branch of a complex biantennary Asn-linked oligosaccharide. *J Biol Chem*. 1984;259:4716–4721.
62. Datta AK, Paulson JC. The sialyltransferase "sialylmotif" participates in binding the donor substrate CMP-NeuAc. *J Biol Chem*. 1995;270:1497–1500.
63. Kochanowski N, Blanchard F, Cacan R, Chirat F, Guedon E, Marc A, Goergen JL. Intracellular nucleotide and nucleotide sugar contents of cultured CHO cells determined by a fast, sensitive, and high-resolution ion-pair RP-HPLC. *Anal Biochem*. 2006;348:243–251.
64. Yurchenco PD, Atkinson PH. Fucosyl-glycoprotein and precursor polls in HeLa cells. *Biochemistry*. 1975;14:3107–3114.
65. Gu X, Wang DI. Improvement of interferon-gamma sialylation in Chinese hamster ovary cell culture by feeding of N-acetylmannosamine. *Biotechnol Bioeng*. 1998;58:642–648.
66. Process Systems Enterprise, Ltd. *gPROMS Introductory User Guideversion 3.3.1* London, UK: Process Systems Enterprise Ltd.; 2009.
67. Quinn P, Griffiths G, Warren G. Density of newly synthesized plasma membrane proteins in intracellular membranes. II. Biochemical studies. *J Cell Biol*. 1984;98:2142–2147.
68. Gilchrist A, Au CE, Hiding J, Bell AW, Fernandez-Rodriguez J, Lesimple S, Nagaya H, Roy L, Gosline SJC, Hallett M, Paiement J, Kearney RE, Nilsson T, Bergeron JJM. Quantitative proteomics analysis of the secretory pathway. *Cell*. 2006;127:1265–1281.
69. Pels Rijcken WR, Overdijk B, Eijnden DH Van, Ferwerda W. The effect of increasing nucleotide-sugar concentrations on the incorporation of sugars into glycoconjugates in rat hepatocytes. *Biochem J*. 1995;305 (pt 3):865–870.
70. Ishida N, Yoshioka S, Chiba Y, Takeuchi M, Kawakita M. Molecular cloning and functional expression of the human Golgi UDP-N-acetylglucosamine transporter. *J Biochem*. 1999;126:68–77.
71. Yoshioka S, Sun-Wada GH, Ishida N, Kawakita M. Expression of the human UDP-galactose transporter in the Golgi membranes of murine Had-1 cells that lack the endogenous transporter. *J Biochem*. 1997;122:691–695.
72. Zhao W, Chen TL, Vertel BM, Colley KJ. The CMP-sialic acid transporter is localized in the medial-trans Golgi and possesses two specific endoplasmic reticulum export motifs in its carboxyl-terminal cytoplasmic tail. *J Biol Chem*. 2006;281:31106–31118.
73. Nakano M, Higo D, Arai E, Nakagawa T, Kakehi K, Taniguchi N, Kondo A. Capillary electrophoresis-electrospray ionization mass spectrometry for rapid and sensitive N-glycan analysis of glycoproteins as 9-fluorenylmethyl derivatives. *Glycobiology*. 2009;19:135–143.
74. Stadlmann J, Pabst M, Kolarich D, Kunert R, Altmann F. Analysis of immunoglobulin glycosylation by LC-ESI-MS of glycopeptides and oligosaccharides. *Proteomics*. 2008;8:2858–2871.
75. Imai-Nishiya H, Mori K, Inoue M, Wakitani M, Iida S, Shitara K, Satoh M. Double knockdown of alpha1,6-fucosyltransferase (FUT8) and GDP-mannose 4,6-dehydratase (GMD) in antibody-producing cells: a new strategy for generating fully non-fucosylated therapeutic antibodies with enhanced ADCC. *BMC Biotechnol*. 2007;7:84.
76. Kochanowski N, Blanchard F, Cacan R, Chirat F, Guedon E, Marc A, Goergen JL. Influence of intracellular nucleotide and nucleotide sugar contents on recombinant interferon-gamma glycosylation during batch and fed-batch cultures of CHO cells. *Biotechnol Bioeng*. 2008;100:721–733.
77. Wong NSC, Wati L, Nissom PM, Feng HT, Lee MM, Yap MGS. An investigation of intracellular glycosylation activities in CHO cells: effects of nucleotide sugar precursor feeding. *Biotechnol Bioeng*. 2010;107:321–336.
78. Lippincott-Schwartz J, Altan-Bonnet N, Patterson GH. Photobleaching and photoactivation: following protein dynamics in living cells. *Nat Cell Biol*. 2003 (Suppl) S7–14.

Manuscript received Jan. 18, 2011, and revision received July 25, 2011.